1   **Midbrain activity supports high-level visual properties in primate temporal cortex**

2

3

4   Amarender R. Bogadhi*[1], Leor N. Katz*[1], Anil Bollimunta[1], David A. Leopold[2,3], Richard

5   J. Krauzlis[1]

6

7   1. Laboratory of Sensorimotor Research, National Eye Institute, National Institutes

8   of Health

9   2. Laboratory of Neuropsychology, National Institute of Mental Health, National

10   Institutes of Health

11   3. Neurophysiology Imaging Facility, National Institute of Mental Health, National

12   Institute of Neurological Disorders and Stroke, National Eye Institute, National

13   Institutes of Health

14

15   * These authors contributed equally

16

17   Corresponding Authors:

18   richard.krauzlis@nih.gov

19   bogadhi.amar@gmail.com

20

21

22

23

24   **Abstract**

25   The evolution of the primate brain is marked by a dramatic increase in the

26   number of neocortical areas that process visual information [1]. This cortical expansion

27   supports two hallmarks of high-level primate vision – the ability to selectively attend to

28   particular visual features [2] and the ability to recognize a seemingly limitless number of

29   complex visual objects [3]. Given their prominent roles in high-level vision for primates, it

30   is commonly assumed that these cortical processes supersede the earlier versions of

31   these functions accomplished by the evolutionarily older brain structures that lie

32   beneath the cortex. Contrary to this view, here we show that the superior colliculus

33   (SC), a midbrain structure conserved across all vertebrates [4], is necessary for the

34   normal expression of attention-related modulation and object selectivity in a newly

35   identified region of macaque temporal cortex. Using a combination of psychophysics,

36   causal perturbations and fMRI, we identified a localized region in the temporal cortex

37   that is functionally dependent on the SC. Targeted electrophysiological recordings in

38   this cortical region revealed neurons with strong attention-related modulation that was

39   markedly reduced during attention deficits caused by SC inactivation. Many of these

40   neurons also exhibited selectivity for particular visual objects, and this selectivity was

41   also reduced during SC inactivation. Thus, the SC exerts a causal influence on high-

42   level visual processing in cortex at a surprisingly late stage where attention and object

43   selectivity converge, perhaps determined by the elemental forms of perceptual

44   processing the SC has supported since before there was a neocortex.

45

46

47   **Main text:**

48   The primate superior colliculus (SC) in the midbrain is crucial for the normal

49   control of visual attention, but whether and how SC activity interacts with cortical

50   processing for attention is controversial [5,6]. As a step toward identifying which areas of

51   cortex might be influenced by the SC, we performed fMRI in monkeys performing

52   attention tasks (figure 1a, b) and identified a novel attention-related region in the floor of

53   the superior temporal sulcus (fSTS) of cortex (figure 1c; [7]). By combining fMRI with and

54   without SC inactivation, we found that the same fSTS region exhibited the largest

55   reduction in attention-related BOLD modulation during the attention deficits caused by

56   SC inactivation (figure 1d; [8]). Relatively little is known about this cortical fSTS region [9-14]

57   and it is unclear why it emerged in fMRI as the primary cortical area dependent on SC

58   activity during the attention task. Our next step was to target this region for extracellular

59   recording (figure 1e) to identify the signals conveyed by neurons and how these signals

60   might depend on superior colliculus activity.

61   We recorded neuronal activity in the fSTS region, before and during SC

62   inactivation, while two monkeys performed the same attention task used in fMRI

63   experiments. In all conditions, monkeys maintained central fixation for the entirety of the

64   trial and reported relevant stimulus changes by releasing a joystick. In the *Attend*

65   condition (figure 1a), monkeys reported a change in the direction of motion of either of

66   two peripheral visual stimuli. In the *Ignore* condition (figure 1b), monkeys ignored the

67   behaviorally irrelevant direction changes in the peripheral stimuli and reported when the

68   central fixation spot dimmed. The magnitude of stimulus change was adjusted such that

69   the task was demanding and animals were at threshold performance – animals correctly

3

70   responded in 73% ± 14% of trials in the *Attend* condition and 62% ± 13% in the *Ignore*

71   condition (mean ± sd of both monkeys, see figure 1a, b for individual performance).

72   The targeted neuronal recordings during the attention task revealed a "hotspot"

73   of attention-related modulation in fSTS (figure 1e). Neurons near the center of the fMRI-

74   identified region tended to fire more in the *Attend* condition than in the *Ignore* condition

75   compared to neurons in adjacent locations (figure 1e). Overall, fSTS neurons displayed

76   strong attention-related modulation (figure 2a, c; Wilcoxon signed-rank test p < 6e-64, n

77   = 380), and the median attention modulation index (AMI = 0.11; supplementary figure 1)

78   was larger than what is typically observed in other areas of visual cortex (AMI = 0.051 in

79   MT and 0.048 in MST [15]).

80   We next tested whether this neuronal response modulation was affected by

81   reversible inactivation of the SC. We confirmed that inactivation of the SC by

82   microinjection of muscimol caused major deficits in attention task performance;

83   consistent with previous findings [16], the deficits were spatially restricted to portions of

84   the visual field contralateral to the injection site (supplementary figures 2-3). We found

85   that the attentional modulation of fSTS neurons was markedly reduced by SC

86   inactivation, unlike neurons in extrastriate visual cortex [15]. The loss of attentional

87   modulation was evident in the population averages of discharge rate over time (figure

88   2a, b), in individual neurons (figure 2c; Wilcoxon rank-sum test, p < 3e-12), across

89   sessions (figure 2d; Wilcoxon signed-rank test, p < 0.002), and was not evident during

90   control injections of saline (supplementary figure 4). Using a traditional attention

91   modulation index (supplementary figure 1), modulation dropped by 45.9% during SC

92   inactivation (from median of 0.11 before to 0.06 during). The reductions in attentional

4

93   modulation cannot be explained by changes in neural spike rate or tuning properties

94   since these were unchanged during SC inactivation (supplementary figure 5). These

95   reductions also cannot be attributed to micro-saccades because the reductions in

96   modulation were also observed in trials without micro-saccades (supplementary figure

97   6). These findings demonstrate that the large attention-related modulation of neurons in

98   fSTS cortex depends on midbrain SC activity.

99   In addition to the attention-related modulation, neurons in fSTS also responded

100   vigorously to the change in motion direction during the attention task (figure 3a). Since

101   correct detection of the change was the crux of the attention task, this change-related

102   activity is also an important feature of fSTS neurons. This change-related activity was

103   also significantly attenuated during SC inactivation, as evident in the average population

104   response to change (figure 3b), in single neurons (figure 3c; Wilcoxon rank-sum test, p

105   < 4e-3), and across sessions (figure 3d; Wilcoxon signed-rank test, p < 0.03). We next

106   quantified how well the trial-by-trial variation in change-related activity predicted the

107   animal's successful detections (a quantity termed *detect probability*). Before SC

108   inactivation, detect probabilities were significantly greater than chance (figure 3g,

109   Wilcoxon signed-rank test, p < 6e-64). During SC inactivation, detect probabilities were

110   substantially reduced for both individual neurons (figure 3g; Wilcoxon rank-sum test, p <

111   3e-4) and experimental sessions (figure 3h; Wilcoxon signed-rank test, p < 0.03).

112   Control saline injections again confirmed that these effects required suppression of SC

113   activity (supplementary figure 7). These reductions in detect probability show that the

114   degree to which fSTS activity can predict animal performance on a trial-by-trial basis

115   also depends on SC activity.

116   The loss of attention-related properties in fSTS neurons during SC inactivation

117   was not specific to the feature of visual motion. Significant reductions in all of the

118   neuronal measures reported – attention-related modulation, change-related modulation,

119   and detect probabilities – were also observed (supplementary figure 8) when the

120   experiments were repeated using a different visual stimulus (a brief pulse of second-

121   order orientation) that was designed such that it cannot be detected using motion

122   energy [8].

123   These results identify the fSTS region as part of a novel circuit for attention

124   control that depends on SC activity. The properties of this control mechanism are

125   different from the well-known mechanisms centered in the prefrontal cortex, which are

126   thought to provide feedback signals to early visual areas that regulate how basic visual

127   features are processed [17]. First, fSTS lies at a later stage in the hierarchy of cortical

128   visual areas [18,19]. Second, the control of fSTS region by the SC is not specific to a

129   particular visual feature (supplementary figure 8). Third, the changes in fSTS caused by

130   SC inactivation omitted two signatures of selective attention typically found in earlier

131   visual areas – neither spike-count correlations nor Fano factor [20,21] showed consistent

132   effects during the attention deficits caused by reversible inactivation (supplementary

133   figure 9).

134   Given the proximity of fSTS to visual form processing areas and the lack of

135   feature specificity in its dependence on SC, we speculated that the SC control of fSTS

136   region might be related to elemental perceptual forms and events rather than the

137   detailed representation of visual features afforded by the expansion of neocortex. To

138   this end, we tested for another visual property that is common in the temporal lobe but

139   usually studied separately from attention – selectivity for visual objects [22-24]. Monkeys

140   passively viewed a stream of briefly (250 ms) flashed images of visual objects within the

141   receptive fields of neurons recorded in the fSTS. To control for low-level visual features,

142   we also included grid- and phase-scrambled versions of the same images randomly

143   intermixed in the stream (figure 4a).

144   About one-third of the neurons we recorded exhibited strong selectivity for

145   particular visual objects. For example, neurons responded vigorously during the

146   presentation of a particular image (e.g. "water bottle"), but not during any of the other

147   intact or scrambled images (figure 4b). Across the population of 303 neurons, 92

148   showed significant selectivity for at least one object (figure 4c), and this selectivity

149   cannot be attributed to attention drawn to particular images, because neurons recorded

150   at the same time showed selectivity for different images (e.g. units #54, #57 & #58 in

151   figure 4b). The rapid rise, strength and prevalence of object selectivity was evident in

152   the population responses (figure 4d) and the distribution of object selectivity values

153   (median = 0.56, significantly greater than 0.5, Wilcoxon signed-rank test, $p < 2e-51$).

154   During SC inactivation, the number of object-selective neurons was substantially

155   reduced from 30.3% (92/303) to 17.89% (51/285) (figure 4c; Chi-square test, $p < 7e-4$).

156   Significant reductions in object-selectivity during SC inactivation were evident in

157   population responses (figure 4d, e) and individual neurons (Figure 4f; Wilcoxon rank-

158   sum test, $p < 4e-4$). The reduction in object-selectivity was consistent across sessions

159   (Figure 4h; Wilcoxon signed-rank test, $p < 0.04$) and monkeys (supplementary figure

160   10). This finding demonstrates that fSTS neurons gain their basic visual object

161   selectivity, in part, through a pathway that involves the superior colliculus.

162   In summary, our findings demonstrate that the primate SC plays a causal role in

163   the cortical processing of visual stimuli through a previously undistinguished patch of

164   cortex in the fSTS. SC activity probably reaches fSTS through the thalamic pulvinar [25-

165   27]. Similar ascending circuits from SC through higher-order thalamus to later stages of

166   visual cortex have been recently described in mice [28-30]. The functions of these circuits

167   from the SC may complement those of the well-known hierarchy of visual pathways

168   starting in the lateral geniculate nucleus of the thalamus [18,19]. We suggest that the

169   cortical visual system might use signals from the SC as a shortcut for rapid object

170   processing: rather than relying on feedforward hierarchical circuits to identify all possible

171   objects in a scene, inputs from the SC might guide the efficient recognition of objects at

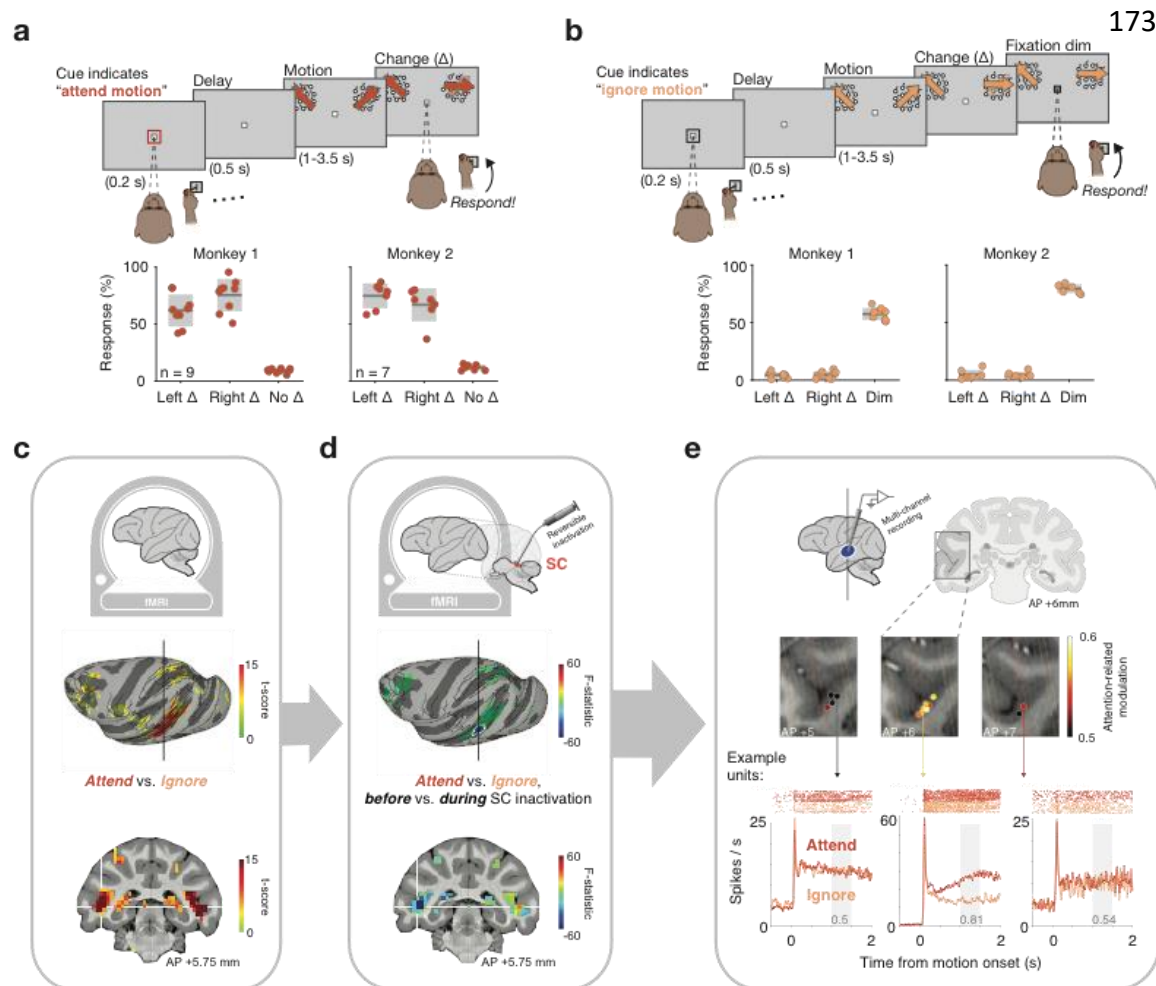172   the specific location deemed most important at that moment.

Figure 1. Identification of a cortical region dependent on SC activity

a. Top: Red cue instructed monkey to attend motion stimulus and report a change in motion direction (Δ). Bottom: response rates for left and right Δ (hits) and "no-Δ" (catch) trials. Individual sessions are plotted over gray box indicating mean ± sd.

b. Top: Black cue instructed monkey to ignore motion-changes and report a dim in fixation spot. Bottom: response rates for left and right Δ (false alarms) and for dim (hits). Same format as a.

c. Functional activations contrasting Attend and Ignore revealed maximal attention-related modulation in the fundus of STS (fSTS).

d. Functional activations with and without SC inactivation identified a circumscribed region (blue colored patch) in fSTS whose modulation was the most dependent on SC activity.

e. Coronal slices of the fSTS are overlaid with average attention modulation across neurons recorded in each location (colored spots). Oblique lines indicate electrode approach. Bottom: Example neuronal responses to *Attend* and *Ignore* conditions from three recording locations and their corresponding modulation values (gray text).
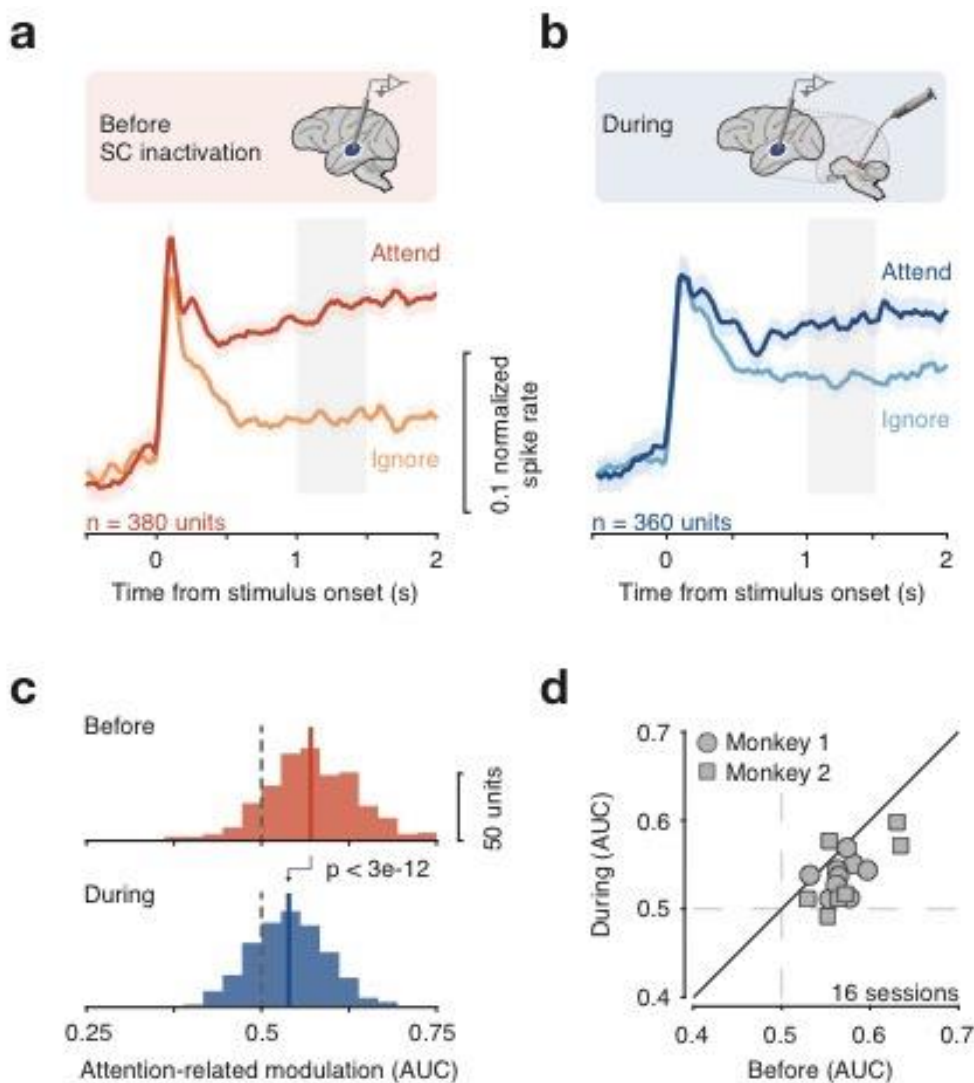
192
193
194
195 **Figure 2. Attention-related modulation in fSTS neurons is dependent on SC**
196 **activity**
197   a-b. Population average of the normalized responses to motion stimulus in *Attend*
198   and *Ignore* conditions before (a) and during (b) SC inactivation. Error bars
199   indicate 68.2% CI. Grey window indicates time period used for computing
200   attention-related modulation.
201   c. Distribution of attention-related modulation values across neurons before and
202   during SC inactivation. Solid and dotted lines indicate median and no modulation
203   respectively.
204   d. Average attention-related modulation across simultaneously recorded neurons
205   within a session (mean ± sd = 23.75 ± 8.72), before and during SC inactivation.
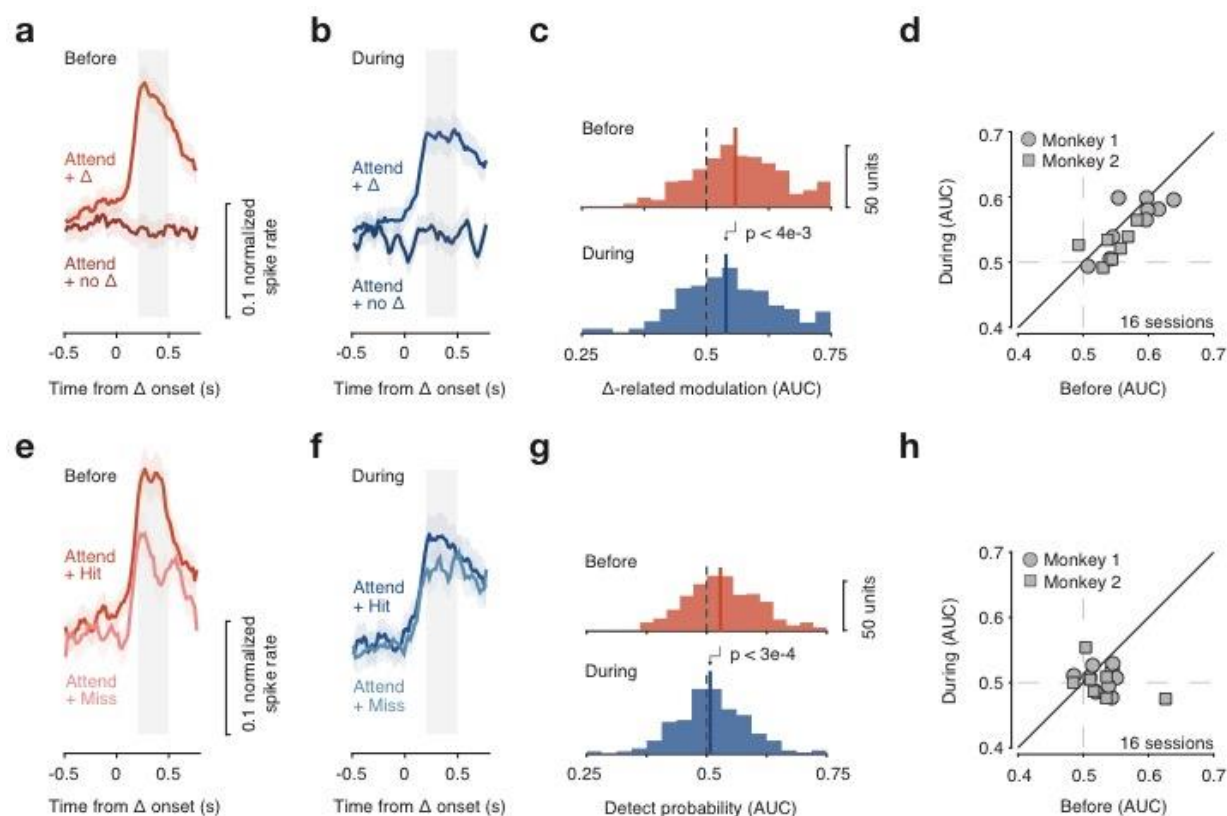
206
207
208

10

Figure 3. Change detection in fSTS neurons is dependent on SC activity

a-b. Population average of the normalized responses to motion-change (Δ) and no-change (no Δ) events in the *Attend* condition before (a) and during (b) SC inactivation. Grey window indicates time period used for computing change-related modulation. Error bars: 68.2% CI.

c. Distribution of change-related modulation values before and during SC inactivation. Solid and dotted lines indicate median and no modulation respectively.

d. Effect of SC inactivation on change-related modulation across sessions.

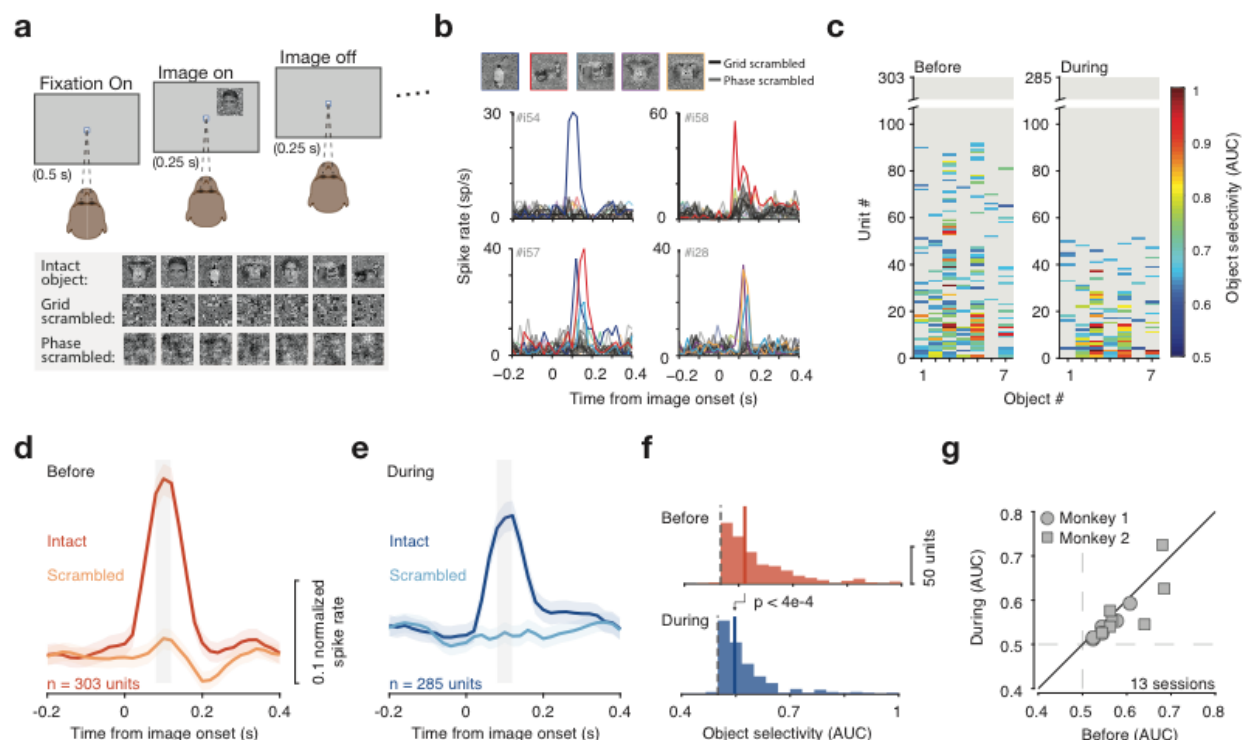e-h. Same conventions as in a-d but comparing hit and miss motion-change trials.

Figure 4. Object selectivity in fSTS neurons is dependent on SC activity

a. Monkeys fixated a central spot while either object, grid-scrambled, or phase-scrambled images were presented.

b. Example neurons that responded selectively to individual object images.

c. Object selectivity values for individual neurons, sorted by number of objects selective for, before and during SC inactivation. Non-significant selectivity (p > 0.05) is shown as grey.

d-e. Population average of normalized responses to the most selective object and the corresponding scrambled object, before (d) and during (e) SC inactivation. Grey window indicates time period used for computing object selectivity. Error bars: 68.2% CI.

f. Distribution of object selectivity values before and during SC inactivation. Solid and dotted lines indicate median and no selectivity respectively.

g. Effect of SC inactivation on object-selectivity across sessions.

241 **References**

242 1.   Kaas, J. H. The evolution of neocortex in primates. *Prog Brain Res* **195,** 91–102
243   (2012).
244 2.   Kastner, S. & Ungerleider, L. G. Mechanisms of visual attention in the human
245   cortex. *Annu Rev Neurosci* **23,** 315–341 (2000).
246 3.   Logothetis, N. K. & Sheinberg, D. L. Visual object recognition. *Annu Rev Neurosci*
247   **19,** 577–621 (1996).
248 4.   May, P. The mammalian superior colliculus: laminar structure and connections.
249   *Prog Brain Res* **151,** 321–378 (2006).
250 5.   Krauzlis, R. J., Lovejoy, L. P. & Zenon, A. Superior colliculus and visual spatial
251   attention. *Annu Rev Neurosci* **36,** 165–182 (2013).
252 6.   Basso, M. A. & May, P. J. Circuits for Action and Cognition: A View from the
253   Superior Colliculus. *Annu Rev Vis Sci* **3,** 197–226 (2017).
254 7.   Bogadhi, A. R., Bollimunta, A., Leopold, D. A. & Krauzlis, R. J. Brain regions
255   modulated during covert visual attention in the macaque. *Sci Rep* **8,** 15237
256   (2018).
257 8.   Bogadhi, A. R., Bollimunta, A., Leopold, D. A. & Krauzlis, R. J. Spatial Attention
258   Deficits Are Causally Linked to an Area in Macaque Temporal Cortex. *Curr Biol*
259   **29,** 726–736.e4 (2019).
260 9.   Desimone, R. & Ungerleider, L. G. Multiple visual areas in the caudal superior
261   temporal sulcus of the macaque. *J Comp Neurol* **248,** 164–189 (1986).
262 10.   Nelissen, K., Vanduffel, W. & Orban, G. A. Charting the lower superior temporal
263   region, a new motion-sensitive region in monkey superior temporal sulcus. *J
264   Neurosci* **26,** 5929–5947 (2006).
265 11.   Rosenberg, A., Wallisch, P. & Bradley, D. C. Responses to direction and
266   transparent motion stimuli in area FST of the macaque. *Vis Neurosci* **25,** 187–195
267   (2008).
268 12.   Mysore, S. G., Vogels, R., Raiguel, S. E., Todd, J. T. & Orban, G. A. The
269   selectivity of neurons in the macaque fundus of the superior temporal area for
270   three-dimensional structure from motion. *J Neurosci* **30,** 15491–15508 (2010).
271 13.   Kilintari, M., Raos, V. & Savaki, H. E. Involvement of the superior temporal cortex
272   in action execution and action observation. *J Neurosci* **34,** 8999–9011 (2014).
273 14.   Ward, M. K., Bolding, M. S., Schultz, K. P. & Gamlin, P. D. Mapping the macaque
274   superior temporal sulcus: functional delineation of vergence and version eye-
275   movement-related activity. *J Neurosci* **35,** 7428–7442 (2015).
276 15.   Zenon, A. & Krauzlis, R. J. Attention deficits without cortical neuronal deficits.
277   *Nature* **489,** 434–437 (2012).
278 16.   Lovejoy, L. P. & Krauzlis, R. J. Inactivation of primate superior colliculus impairs
279   covert selection of signals for perceptual judgments. *Nat Neurosci* **13,** 261–266
280   (2010).
281 17.   Squire, R. F., Noudoost, B., Schafer, R. J. & Moore, T. Prefrontal contributions to
282   visual selective attention. *Annu Rev Neurosci* **36,** 451–466 (2013).
283 18.   Felleman, D. J. & Van Essen, D. C. Distributed hierarchical processing in the
284   primate cerebral cortex. *Cereb Cortex* **1,** 1–47 (1991).

285   19.   Hilgetag, C. C., O'Neill, M. A. & Young, M. P. Hierarchical organization of
286   macaque and cat cortical sensory systems explored with a novel network
287   processor. *Philos Trans R Soc Lond B Biol Sci* **355,** 71–89 (2000).
288   20.   Cohen, M. R. & Maunsell, J. H. R. Attention improves performance primarily by
289   reducing interneuronal correlations. *Nat Neurosci* **12,** 1594–1600 (2009).
290   21.   Mitchell, J. F., Sundberg, K. A. & Reynolds, J. H. Spatial attention decorrelates
291   intrinsic activity fluctuations in macaque area V4. *Neuron* **63,** 879–888 (2009).
292   22.   Rolls, E. T. Functions of the primate temporal lobe cortical visual areas in
293   invariant visual object and face recognition. *Neuron* **27,** 205–218 (2000).
294   23.   Tsao, D. Y., Freiwald, W. A., Knutsen, T. A., Mandeville, J. B. & Tootell, R. B. H.
295   Faces and objects in macaque cerebral cortex. *Nat Neurosci* **6,** 989–995 (2003).
296   24.   Hung, C. P., Kreiman, G., Poggio, T. & Dicarlo, J. J. Fast readout of object identity
297   from macaque inferior temporal cortex. *Science* **310,** 863–866 (2005).
298   25.   Harting, J. K., Huerta, M. F., Frankfurter, A. J., Strominger, N. L. & Royce, G. J.
299   Ascending pathways from the monkey superior colliculus: an autoradiographic
300   analysis. *J Comp Neurol* **192,** 853–882 (1980).
301   26.   Boussaoud, D., Desimone, R. & Ungerleider, L. G. Subcortical connections of
302   visual areas MST and FST in macaques. *Vis Neurosci* **9,** 291–302 (1992).
303   27.   Dominguez-Vargas, A.-U., Schneider, L., Wilke, M. & Kagan, I. Electrical
304   Microstimulation of the Pulvinar Biases Saccade Choices and Reaction Times in a
305   Time-Dependent Manner. *J Neurosci* **37,** 2234–2257 (2017).
306   28.   Beltramo, R. & Scanziani, M. A collicular visual cortex: Neocortical space for an
307   ancient midbrain visual structure. *Science* **363,** 64–69 (2019).
308   29.   Bennett, C. *et al.* Higher-Order Thalamic Circuits Channel Parallel Streams of
309   Visual Information in Mice. *Neuron* **102,** 477–492.e5 (2019).
310   30.   Tohmi, M., Meguro, R., Tsukano, H., Hishida, R. & Shibuki, K. The
311   extrageniculate visual pathway generates distinct response properties in the
312   higher visual areas of mice. *Curr Biol* **24,** 587–597 (2014).
313

Methods

Animals

Two adult male rhesus monkeys (*Macaca mulatta*) weighing 7-9 kg were used in the study. All procedures and animal care were approved by the National Eye Institute Animal Care and Use Committee and complied with the Public Health Service Policy on the humane care and use of laboratory animals. We surgically implanted plastic head-posts and electrophysiology chambers, under isoflurane and aseptic conditions, to access the SC and the fundus of the STS (fSTS). The placement of the fSTS chamber was guided by previously obtained functional imaging results [8], and we targeted the fSTS region in different hemispheres across the two monkeys. Both monkeys were trained on an attention task (figure 1a, b), a visually guided saccade task (for mapping the affected region during SC inactivation, supplementary figure 2), an object tuning task (figure 4a), and several other passive fixation tasks (for mapping spatial receptive fields and direction tuning of single neurons).

Experimental apparatus

Animals were seated and head-fixed in a primate chair (Crist Instrument Inc., Hagerstown, MD, and custom-built) inside a darkened booth at a distance of 48 cm from a VIEWPixx display (VPixx Technologies, Saint-Bruno, QC Canada) with a 1920 x 1200 resolution ($\sim 60°$ x $38°$) and 100Hz frame-rate. Stimuli were presented on the VIEWPixx display that was controlled by a mid-2010 Mac Pro (Apple Inc., Cupertino, CA) running MATLAB (The Mathworks, Natick, MA) with the Psychophysics Toolbox extensions [32]. The background luminance of the screen across all tasks was 14 cd/m^2. Eye position was recorded using an EyeLink 1000 infrared eye-tracking system (SR Research Ltd.,

337   Ottowa, Ontario, Canada); this signal was monitored online to ensure strict fixation

338   within a 2° fixation window during all tasks. The primate chairs were equipped with a

339   single axis joystick (CH Products, model HFX-10) that the monkeys used to report

340   relevant stimulus changes during the attention task. Joystick presses and releases were

341   detected by a change in voltage signal. All experiments were controlled using a

342   modified version of PLDAPS [33].

343   Electrophysiology recording

344   Neuronal and behavioural signals (e.g. eye position, joystick) were acquired by

345   an Omniplex system (Plexon Inc., Dallas, Texas). Neuronal signals were recorded using

346   a 24-channel linear array (V-probes, Plexon Inc., Dallas, Texas) that was introduced

347   into the fSTS region by a custom built motorized micro-drive. Figure 1e shows coronal

348   sections of fSTS region overlaid with colored spots representing average attention-

349   related modulation (see below) of all neurons recorded in that grid hole. AP and ML

350   location of the colored spots were determined by the grid hole, depth was determined

351   as the average depths across recording sessions in that grid hole. In additional

352   sessions, we recorded a few millimeters away from the 'hotspot' and found either non-

353   standard responses to the stimulus onset or no response at all (supplementary figure

354   11), indicating that our region of interest in the fSTS is circumscribed.

355   Entry into the target fSTS region was confirmed based on depth measurements

356   compared to the MRI slices (figure 1e), and changes in neural activity observed during

357   transitions from gray matter in the dorsal bank of the STS to sulcus, and from sulcus to

358   gray matter in the target region of the fSTS. Upon entry into the target region we

16

359   allowed the V-probe to settle and the neuronal activity to stabilize (~1 hour) before

360   beginning the experimental session.

361   Each session began with an online mapping of spatial receptive fields to optimize

362   stimulus placement for the subsequent tuning and attention tasks. Following the

363   mapping, we collected neuronal responses during the direction tuning, attention, and

364   object tuning tasks. At the end of the "before SC inactivation" set of tasks, we reversibly

365   inactivated SC, and continued collecting data for the "during SC inactivation" set of

366   tasks, starting with the attention task, followed by the tuning and receptive field mapping

367   tasks. Overall, we performed 22 experimental sessions with SC inactivation: 16 with

368   motion-change detection stimulus (9 in monkey #1; 7 in monkey #2); 6 with orientation

369   pulse detection stimulus (in monkey #1), and 8 additional control sessions of saline

370   injection and sham with the motion-change detection stimulus (monkey #1).

371   <u>Receptive field mapping task</u>

372   Spatial receptive fields of fSTS neurons were mapped in each experimental

373   session before and during SC inactivation, while monkeys performed a passive fixation

374   task. Monkeys started each trial by fixating a central square spot (0.21° wide; green

375   colour). Following 0.5 s of fixation, a random dot motion stimulus was presented briefly

376   (0.25 s on and 0.25 s off) within a circular aperture (3° radius) at 100% coherence. The

377   stimulus was presented at locations drawn randomly from an XY grid (5° spacing,

378   covering the display) and at locations selected by the experimenter based on the

379   neuronal responses. The direction of the motion stimulus was pseudo-randomized

380   across stimulus presentations. Each trial lasted for 4 seconds and consisted of 6

381   stimulus presentations. Monkeys were required to maintain fixation within a 2° window

17

382   for the full duration of the trial to receive a reward. We collected an average of 552

383   (before) and 522 (during) presentations in each experimental session.

384   After receptive field mapping, a location was selected by the experimenter which

385   maximized the spatial overlap of receptive fields across the recording channels. This

386   selected location was thereafter fixed for all subsequent tasks: the direction tuning task,

387   the object tuning task, and the attention task, before and during SC inactivation. Overall,

388   locations used ranged between 8 – 14° eccentricity across all sessions.

389   Direction tuning task

390   Direction tuning properties of fSTS neurons were mapped in each experimental

391   session before and during SC inactivation, while animals performed a passive fixation

392   task. The fixation task was similar to the receptive field mapping task, except that each

393   brief motion stimulus presentation (0.25 s on and 0.25 s off) was presented at the fixed

394   visual field location. Random dot motion was presented at 100% coherence and the

395   direction of motion was selected pseudo-randomly on each stimulus presentation from

396   one of the 12 directions (equally spaced from 0 to 360 degrees). A 0% coherence

397   stimulus was also included. Each trial lasted for 4 seconds and consisted of 6 stimulus

398   presentations. Overall, we collected an average of 40 (before) and 36 (during)

399   presentations per motion direction in each experimental session.

400   Object tuning task

401   Monkeys performed a passive fixation task similar to the direction tuning task,

402   except that the motion stimulus was replaced with static images containing objects

403   (visual forms) and their corresponding grid- and Fourier phase-scrambled versions

404   (figure 4a). A total of 21 unique images were used (7 object, 7 grid-scrambled and 7

18

405   phase-scrambled images) and all object images were corrected for luminance

406   histogram and Fourier spectra using SHINE toolbox [34], before generating their

407   corresponding scrambled versions. Each image was presented briefly (0.25 s on and

408   0.25 s off) at the fixed location selected previously. Each trial lasted 4 seconds and

409   consisted of 6 image presentations. Overall, we collected an average of 49 (before) and

410   40 (during) presentations per image in each experimental session.

411   <u>Attention task</u>

412   The attention task consisted of two main conditions: *Attend* and *Ignore* (figure 1a,

413   b), plus two control conditions, *Attend Single Patch* and *Baseline*. In all task conditions,

414   monkeys initiated the trial by pressing the joystick down and fixating a central square

415   spot (50 cd/m^2). Following 0.3 s of fixation, a cue in the form of a colored square outline

416   was flashed around the central fixation spot for 0.2 s. The width of the fixation spot was

417   0.21° and the width of the cue was 0.35°. The color of the cue instructed the monkeys to

418   attend or ignore the peripheral motion stimuli and detect the relevant events. In the

419   *Attend* and *Attend Single Patch* trials, the color of the central cue was red, indicating

420   that the relevant event was a direction-change in the peripheral motion stimulus

421   (detailed below). In the *Ignore* and *Baseline* trials, the color of the central cue was black,

422   indicating that direction-change in the peripheral stimulus was irrelevant and the

423   luminance change in the fixation spot was relevant. In all conditions, monkeys were

424   required to maintain central fixation within a 2° fixation window for the full duration of the

425   trial. All four task conditions were presented in a block design where each condition was

426   presented once (in pseudo-random order) before advancing to the next block. Each

427   block consisted of 150 trials: 54 *Attend*; 54 *Ignore;* 30 *Attend Single Patch;* and 12

428   *Baseline*. Monkeys completed an average of 5 blocks before SC inactivation and 4

429   blocks during inactivation across 16 sessions. The sequences of events in each

430   condition are presented below.

431   In *Attend* trials, following 0.5 s after cue offset, two random-dot motion stimuli

432   appeared on either side of the fixation spot in the contralateral and ipsilateral hemi-

433   fields, symmetric to the vertical meridian. The location of the contralateral stimulus

434   matched the location from mapping tasks (see Receptive field mapping section).

435   Overall, location eccentricity ranged between 8 – 14° across sessions. On 77.7% of

436   *Attend* trials, one of the motion stimuli changed direction during 1-3.5 s after stimulus

437   onset (uniform probability), and the monkeys responded by releasing the joystick within

438   0.3 – 0.8 s to receive a reward. On the remaining 22.3% trials, there was no stimulus

439   change and monkeys were rewarded for continuing to hold the joystick pressed ("catch

440   trials").

441   In *Ignore* trials, the peripheral motion stimuli and task sequence were identical to

442   those in the *Attend* trials, but the monkeys were rewarded for ignoring the peripheral

443   stimuli, and instead, responded to a change in fixation spot luminance (decrease of 1-2

444   cd/m^2 across sessions). On 77.7% of *Ignore* trials, the fixation spot luminance change

445   occurred during 1–3.5 s after stimulus onset (uniform probability) and monkeys

446   responded by releasing the joystick within 0.3 – 0.6 s to receive a reward. On the

447   remaining 22.3% of trials, the fixation spot luminance remained unchanged, and

448   monkeys were rewarded for continuing to hold the joystick pressed ("catch trials").

449   Independent of the luminance change, on 66.6% of the trials, one of the two motion

20

450   stimuli changed direction and the monkeys were rewarded for ignoring the motion

451   direction-change and responding to the change in the fixation spot luminance.

452   *Attend Single Patch* trials were identical to *Attend* trials, with only one of the two

453   motion stimuli presented on any given trial. The stimulus was presented either at the

454   same contralateral or ipsilateral location on equal number of trials.

455   *Baseline* trials were identical to *Ignore* trials, except that no peripheral stimulus

456   was presented. In this condition, monkeys were simply required to detect a change in

457   fixation spot luminance.

458   Random dot motion stimulus

459   Each random dot motion stimulus consisted of moving dots presented in a

460   circular 3° radius aperture. The motion direction of each dot was drawn from a normal

461   distribution with a mean value of 30° above horizontal (in all but one session) and a

462   standard deviation of 16°, to be consistent with the previously performed fMRI study [8].

463   The lifetime (10 frames, 100 ms), density (25 dots/$^\circ{}^2$/s), and speed of the dots (15 °/s)

464   were held constant. Luminance of each moving dot in the motion patches was 50 cd/m^2.

465   The change in direction of motion (Δ) ranged from 0.75 to 1.25 standard deviations of

466   mean motion direction across monkeys and sessions.

467   Attention tasks: Orientation-pulse detection

468   In separate sessions, monkey 1 performed a modified version of attention task

469   with the same conditions (*Attend, Ignore, Attend Single Patch, Baseline*), where random

470   dot motion stimulus was replaced with dynamic white noise stimulus and motion-change

471   event was replaced with a brief (0.5 s) second-order orientation pulse. In the *Attend* and

472   *Attend Single Patch* conditions, the monkey reported the orientation pulse event by

21

473   releasing the joystick within 0.3 - 0.8 s to get a reward, whereas in the *Ignore* condition,

474   monkey ignored the orientation pulse event and reported the luminance decrease in the

475   fixation spot by releasing the joystick within 0.3 - 0.6 s to get a reward. We collected an

476   average of 6 blocks before SC inactivation and 5 blocks during SC inactivation across 6

477   sessions.

478   The white noise stimulus had a diameter of 6^0 and consisted of checks, each the

479   size of a pixel, dynamically changing luminance on every frame at random, with

480   luminance values ranging from 8 to 84 cd/m^2. The second-order orientation stimulus

481   was generated by briefly (0.5 s) modulating the contrast of a white noise stimulus with a

482   2-dimensional sinusoid, whose spatial frequency and orientation was 0.7 cycles/deg

483   and 90^0 respectively. Importantly, the mean luminance of the stimulus (38 cd/m^2) was

484   held constant throughout its presentation and was constant across every band in the

485   oriented grating. We refer to this as a second-order orientation stimulus, because the

486   visibility of the oriented grating was due to local differences in contrast, not luminance,

487   and we confirmed that the orientation pulse contained no change in motion energy [8].

488   Reversible inactivation

489   Reversible inactivation of the intermediate layers of the SC (n = 22; monkey #1

490   (left hemisphere): 15, monkey #2 (right hemisphere): 7) was done by injecting muscimol

491   (0.3-0.5 µl; 5 mg/ml) based on methods described previously [16]. All candidate sites were

492   first identified by neuronal recordings and electrical stimulation prior to the muscimol

493   inactivation experiment. Injections were done using a custom-made apparatus [35] using

494   an injection pump (Legato, KD Scientific) at a constant rate of 0.05 µl/min. For saline

495   controls, the same volumes were injected at the same locations in the intermediate

496   layers of the SC at the same rates.

497   <u>Mapping of the impaired visual field</u>

498   Thirty minutes after the end of the muscimol injection, we used a visually guided

499   saccade task to map the affected visual field using methods described previously [16]. We

500   measured the peak velocity for saccades made to targets at different visual field

501   locations before and during inactivation. The locations at which saccade peak velocities

502   were reduced indicated the locus and the extent of the affected visual field

503   (supplementary figure 2).

504   <u>Electrophysiology analysis</u>

505   Electrophysiological data obtained from the linear arrays were sorted offline into

506   single neurons using the *kilosort* algorithm followed by a manual curation in the *phy*

507   software [36]. For analyses related to attention tasks, we included single neurons with an

508   average trial firing rate greater than 1 spike/s in both *Attend* and *Ignore* blocks. The trial

509   firing rate of a neuron was computed as total spikes over the full duration of trial divided

510   by the trial duration. This resulted in inclusion of 380/563 and 360/529 for the before

511   and during conditions, respectively.

512   For each neuron, mean peri-stimulus time histogram (PSTH) was computed by

513   binning spike times in 10ms non-overlapping bins (figure 1e, figure 4b). To compute the

514   average population response in different tasks and epochs (figures 2, 3, 4), we

515   normalized the mean PSTH of each neuron by its peak activity at the stimulus onset in

516   the corresponding task and averaged the normalized PSTHs across all units, followed

517   by a smoothing operation with a 5-point moving average.

23

518   *Attention-related modulation*: We used spike counts in the *Attend* and *Ignore*

519   conditions during the delay period (1 – 1.5 s after stimulus onset, grey window in figure

520   2a, b) as signal and noise respectively to compute the area under the receiver operator

521   characteristic curve (AUC). This AUC value determined a neuron's attention-related

522   modulation. To evaluate the effect of SC inactivation on attention-related modulation we

523   computed the distributions of AUC values before and during SC inactivation (figure 2c).

524   We also computed the traditional attention-related modulation index (AMI) as $\frac{\mu_A - \mu_I}{\mu_A + \mu_I}$,

525   where μ_A is the average spike count during the delay period (1 – 1.5 s after stimulus

526   onset) in *Attend* condition and μ_I is the average spike count in *Ignore* condition. The

527   effects reported in this manuscript do not depend on whether we use our attention-

528   related modulation AUC measure or AMI (supplementary figure 1).

529   *Fano factor index and neural correlations*: In the same epoch as attention-related

530   modulation (1 – 1.5 s after stimulus onset, grey window in figure 2a, b), we computed

531   fano-factor index and neuronal correlation index for each neuron. Fano-factor index was

532   computed as $\frac{f_A - f_I}{f_A + f_I}$, where f_A is the fano-factor during *Attend* and f_I is the fano-factor

533   during *Ignore*; f_A was computed as $\frac{\sigma_A}{\mu_A}$, where σ_A was the variance in spike count during

534   *Attend* condition (supplementary figure 9). Neuronal correlation index was computed as

535   the difference in inter-neuronal spike count correlations during *Attend* and *Ignore*. Spike

536   count correlation between a pair of neurons was computed as a Pearson's correlation

537   coefficient (MATLAB). Overall, we computed correlations for 4856 pairs of neurons

538   before SC inactivation and 4341 pairs during SC inactivation (supplementary figure 9).

539   *Change-related modulation*: To compute an AUC value that determined a

540   neuron's change-related modulation in activity we used spike counts in the *Attend*

24

541   condition for change trials and no-change trials, during the post-change period (0.2 –

542   0.5 s epoch following the change, grey window in figure 3a, b).

543   *Detect probability*: To compute an AUC value for each neuron's detect probability

544   [37] we compared spike counts in the *Attend* condition for change trials, when the monkey

545   successfully detected a stimulus change ("hit") to when the monkey failed to detect a

546   stimulus change ("miss"), during the post-change period (0.2 – 0.5 s epoch following the

547   change, grey window in figure 3e, f).

548   *Object selectivity*: To compute an AUC value for each neuron's object selectivity

549   in the object-tuning task, we used spike counts for the object image compared to the

550   corresponding scrambled version of the image during the 0.08 – 0.12 s epoch after the

551   image onset (grey window in figure 4d, e).

552

553

554   **Data Availability**

555   The datasets generated during and/or analysed during the current study are available

556   from the corresponding author on reasonable request.

557

558   **Acknowledgments:**

563

564 **Author Contributions**

565 All authors designed the experiments. A.R.B., L.N.K., and A.B. conducted experiments

566 and collected the data. A.R.B. and L.N.K analyzed the data. All authors interpreted the

567 results. R.J.K., A.R.B. and L.N.K. wrote the manuscript.

568

569 **Competing interests:** The authors declare no competing interests.

570

571

572 31. Lowet, E. *et al.* Enhanced Neural Processing by Covert Attention only during
573   Microsaccades Directed toward the Attended Stimulus. *Neuron* **99,** 207–214.e3
574   (2018).
575 32. Brainard, D. H. The Psychophysics Toolbox. *Spat Vis* **10,** 433–436 (1997).
576 33. Eastman, K. M. & Huk, A. C. PLDAPS: A Hardware Architecture and Software
577   Toolbox for Neurophysiology Requiring Complex Visual Stimuli and Online
578   Behavioral Control. *Front Neuroinform* **6,** 1 (2012).
579 34. Willenbockel, V. *et al.* Controlling low-level image properties: the SHINE toolbox.
580   *Behavior research methods* **42,** 671–684 (2010).
581 35. Chen, L., Goffart, L. & Sparks, D. A simple method for constructing
582   microinjectrodes for reversible inactivation in behaving monkeys. *J Neurosci*
583   *Methods* **107,** 81–85 (2001).
584 36. Pachitariu, M., Steinmetz, N. A., Kadir, S. N., Carandini, M. & Harris, K. D. Fast
585   and accurate spike sorting of high-channel count probes with KiloSort. *Advances*
586   *in Neural Information Processing Systems …* 4448–4456 (2016).
587 37. Cook, E. P. & Maunsell, J. H. R. Attentional modulation of behavioral performance
588   and neuronal responses in middle temporal and ventral intraparietal areas of
589   macaque monkey. *J Neurosci* **22,** 1994–2004 (2002).
590
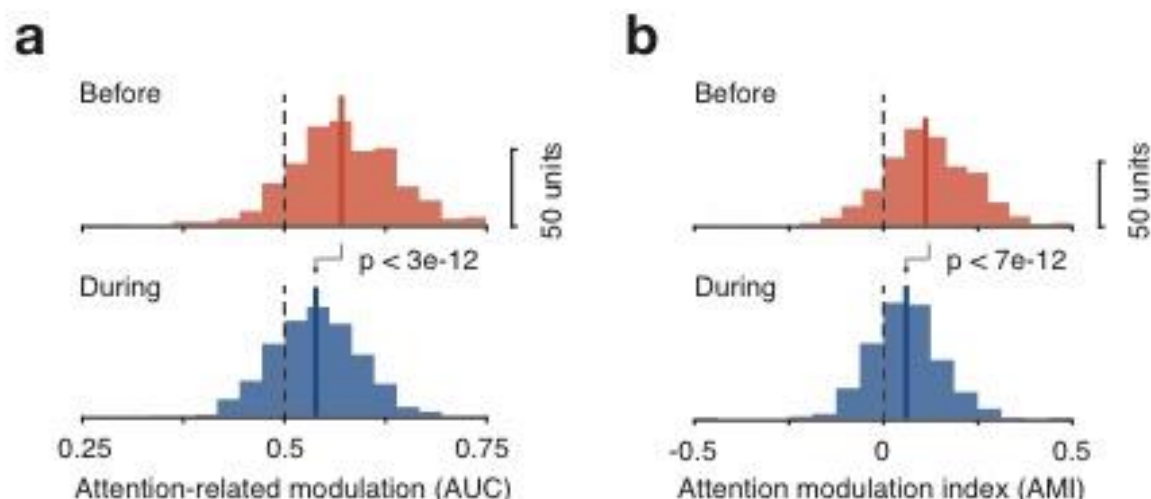
591
592
593 **Supplementary Figure 1. Effect of SC inactivation on attention-related modulation**
594 **in fSTS is consistent across different methods of quantification**
595   a.   Distribution of area under the receiver operator curve (AUC) values quantifying
596   attention-related modulation (see Methods) before (top) and during SC
597   inactivation (bottom) (Same as figure 2c).
598   b.   Distribution of attention modulation index (AMI) values quantifying attention-
599   related modulation (see Methods) before (top) and during SC inactivation
600   (bottom). The difference in distributions is highly significant (see p-values on plot)
601   and similar in both the AUC and AMI cases.
602
603

27

604
605
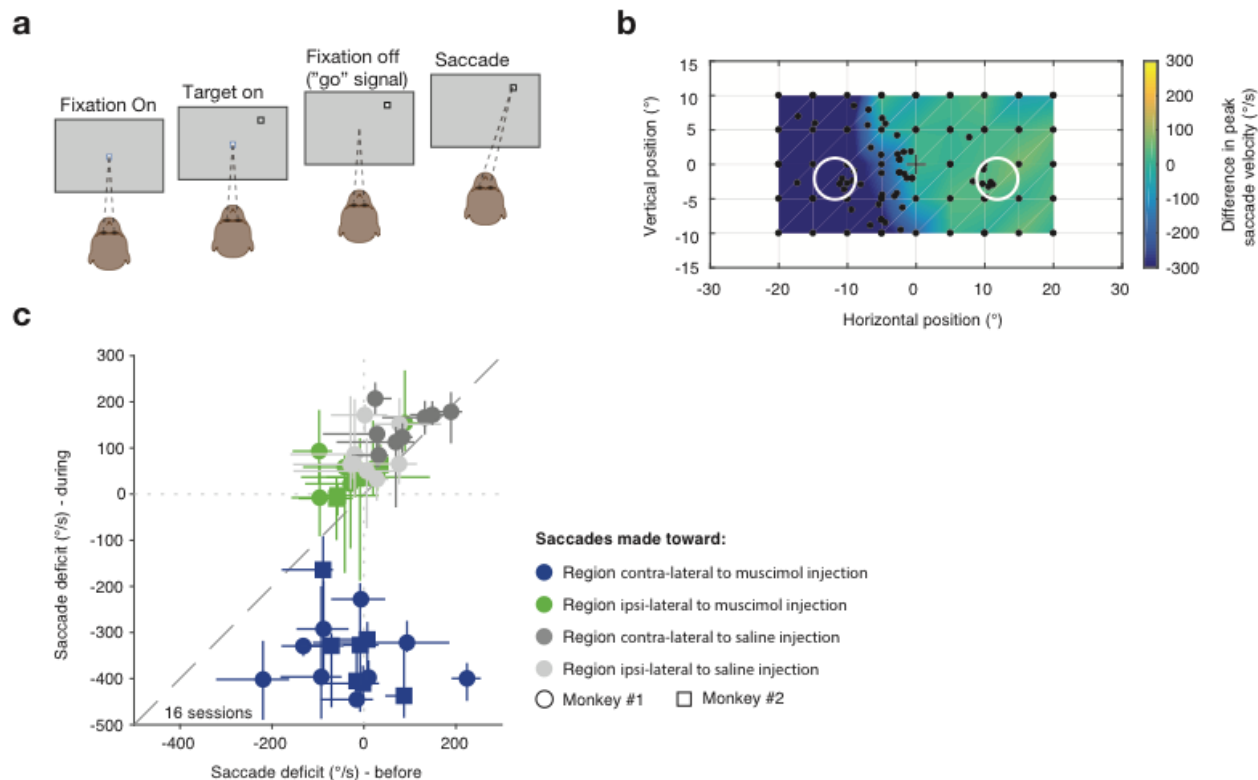
Supplementary Figure 2. SC inactivation was confirmed using a visually guided saccade task

a. Sequence of events in the visually guided saccade task. Following fixation of a central spot, a saccade target was presented at a visual field location. The subject is rewarded for successfully making a saccade to the target upon fixation offset (see methods).

b. A visual field map of saccadic deficit induced by SC inactivation in an example session. The difference between during and before SC inactivation saccade peak velocities is plotted for a large number of sampled targets in space. White circles represent the location of the motion stimulus used in the attention task that followed the visually guided saccade task.

c. Summary of saccade deficit in the contralateral and ipsilateral stimulus locations (white circles in b) before and during injection for muscimol (SC inactivation) and saline injection sessions.

620
621

28
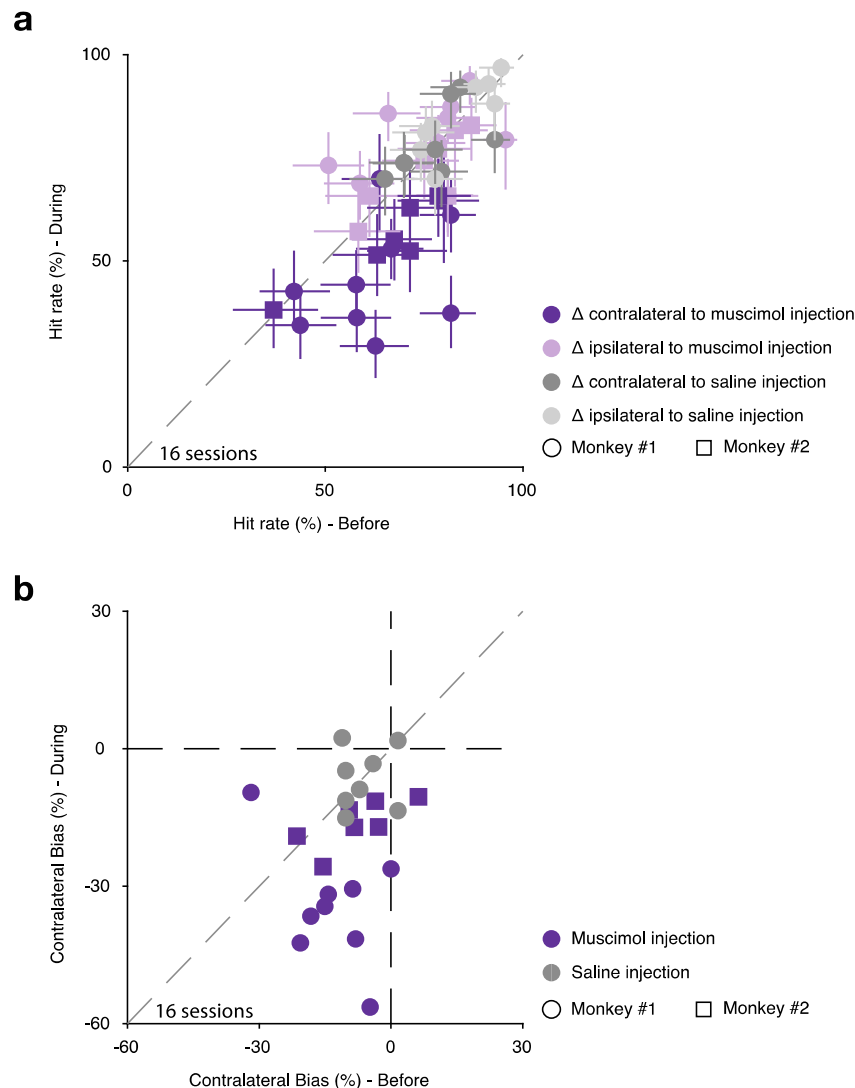
Supplementary Figure 3. Behavioral deficits in the attention task during SC inactivation

The percentage of correctly detected motion-direction changes (hit rate) in the contralateral (affected) visual hemifield was significantly reduced during SC inactivation compared to performance in the ipsilateral (unaffected) visual hemifield (Wilcoxon signed-rank test, $p < 5e-04$) and to performance in the contralateral hemifield before inactivation (Wilcoxon signed-rank test, $p < 0.002$).

a. The successful detection of a change (Δ) in motion direction (hit rate) in the *Attend* condition before SC inactivation vs. during, for when the change occurred in either the contralateral or ipsilateral stimulus, across all muscimol and saline injection sessions.

b. The difference in hit rate between contralateral and ipsilateral motion direction changes in the *Attend* condition (termed "contralateral bias"), before SC inactivation vs. during, across all muscimol and saline injection sessions (same data as in a).
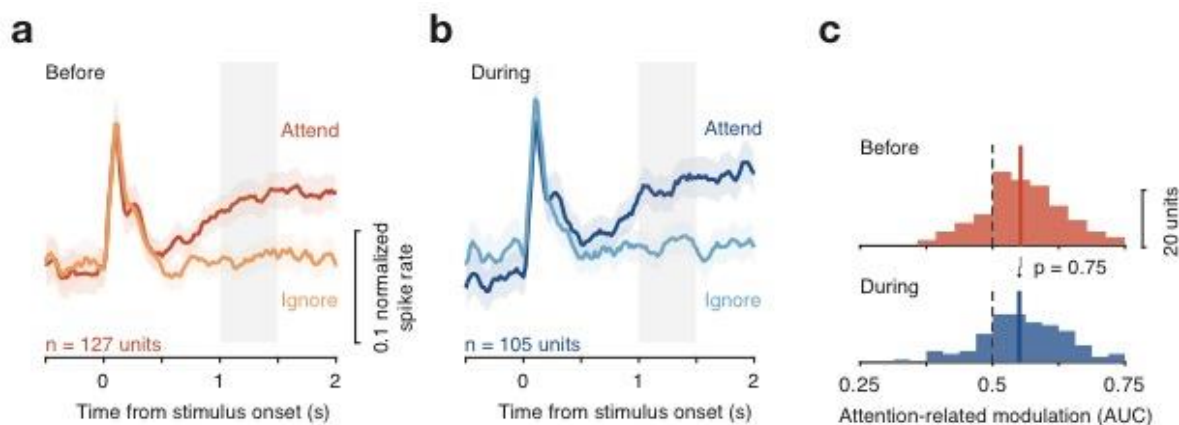
638
639
Supplementary Figure 4. Saline and sham injections had no effect on attention-related modulation in fSTS

a-c. Attention-related modulation before and during saline/sham injections (same format as figure 2a-c).

644
645
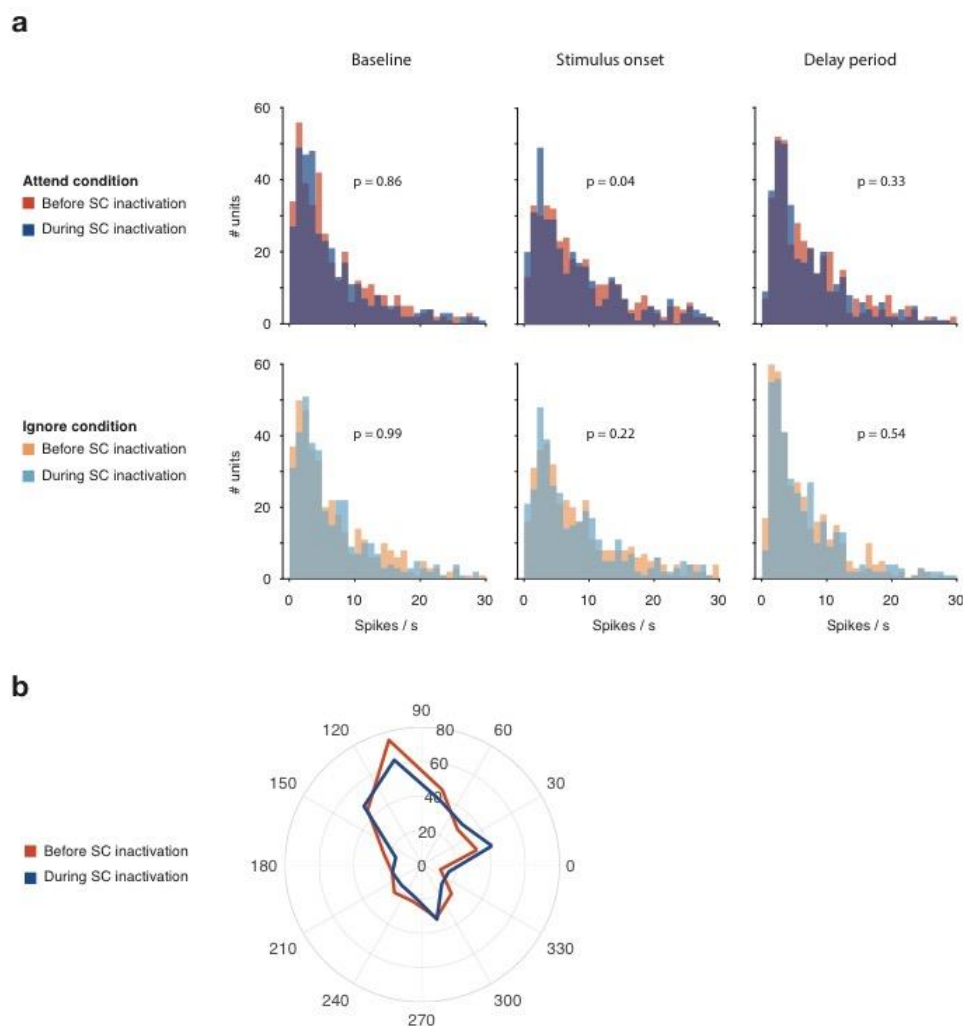
Supplementary Figure 5. SC inactivation did not affect neuronal firing rate or direction tuning

a. Spike rate was computed in three key epochs of *Attend* and *Ignore* conditions: baseline (0.12-0.8s before stimulus onset); stimulus onset (0.8-0.12s after stimulus onset); delay period (1-1.5s after stimulus onset). The distributions of spike rates before and during SC inactivation are shown in the three epochs (up to 30sp/s for visualization) of *Attend* (top) and *Ignore* (bottom) conditions. p-values comparing median firing rate before and during SC inactivation (Wilcoxon rank-sum test) are noted on individual panels.

b. Preferred direction of each neuron was obtained using the direction tuning task (see Methods). Histogram of preferred directions across the fSTS population of neurons, before and during SC inactivation, is plotted in polar coordinates. Radial measure represents number of neurons with the corresponding preferred direction.

31
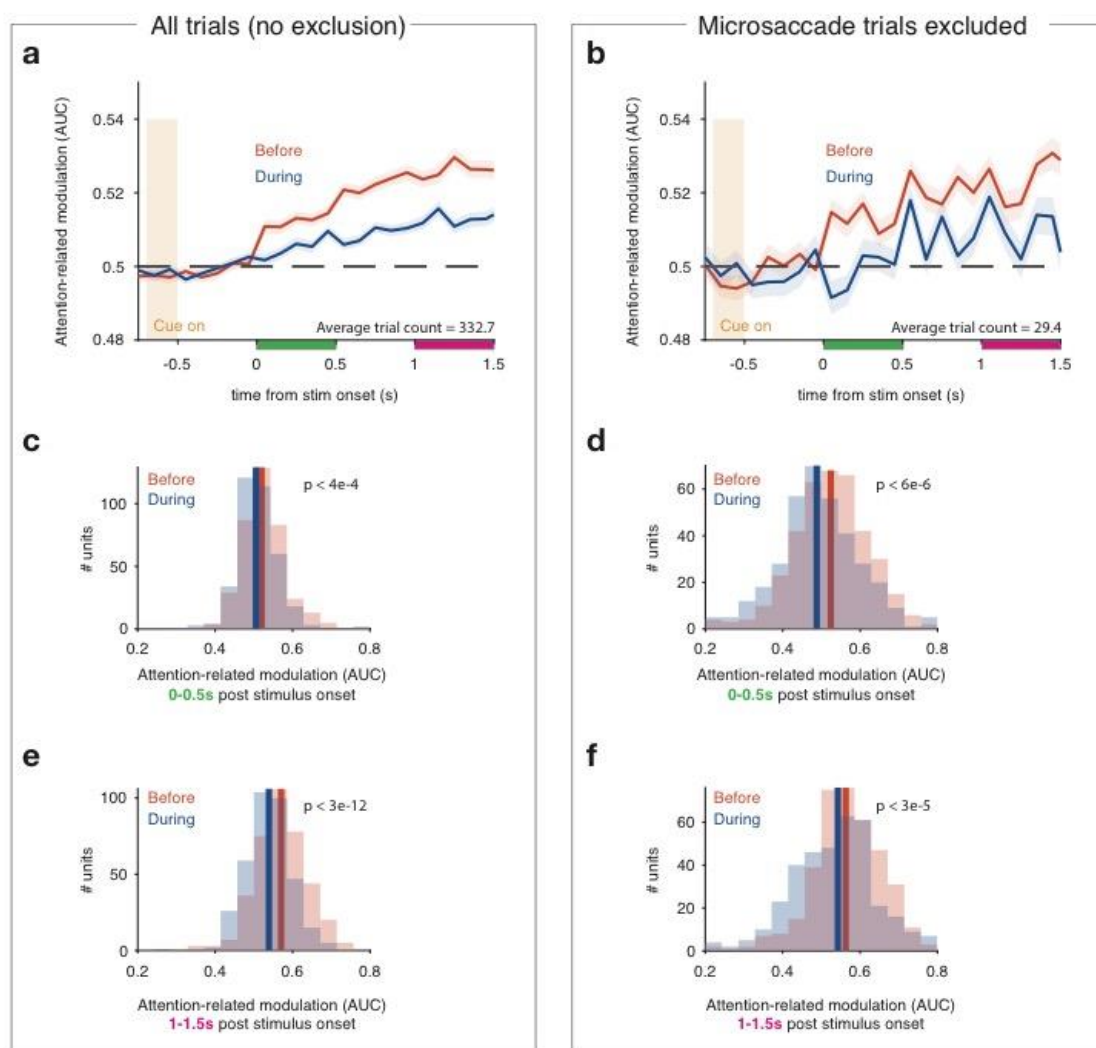
662
663
Supplementary Figure 6. Effect of SC inactivation on attention-related modulation
in fSTS cannot be attributed to microsaccades

A recent study [31] reported that attention-related modulation in visual cortex occurs
only following a microsaccade in the direction of the cued location. To determine
the influence microsaccades might have had on our results, we detected all
microsaccades during the full duration of a trial (amplitude: mean ± sd = 0.42° ±
0.2°) and excluded trials in which a microsaccade occurred anywhere from cue
onset to the end of the time window in which we measured attention-related
modulation (1-1.5s post stimulus onset; figure 2). Excluding trials with
microsaccades anywhere from cue onset until the end of this 1-1.5s window
(magenta box under x-axis in a, b) resulted in too few trials per neuron to
compute an AUC (mean ± sd = 4.83 ± 5.85). The earliest time window that could
be used for this analysis while still yielding sufficient trials for statistical power
was the 0-0.5s window aligned to stimulus onset (green box under x-axis in a, b).
By measuring attention-related modulation in this 0-0.5s window on trials with no

679   microsaccade from cue onset until the end of this 0-0.5s time window, before and
680   during SC inactivation, we show that the effect of SC inactivation on attention-
681   related modulation in fSTS cannot be attributed to microsaccades.

682 a-b. Time-course of attention-related modulation before and during SC inactivation,
683   computed on all trials (a) and on trials with no microsaccade from cue onset to
684   0.5s post stimulus onset (b). Even without microsaccades from cue onset to 0.5s
685   post stimulus (panel b), the attention-related modulation is significant following
686   stimulus onset, and is reduced during SC inactivation.

687 c-d. Distribution of attention-related modulation values before and during SC
688   inactivation, computed in the 0-0.5s time window (green box under x-axis in a, b),
689   on all trials (c) and trials with no microsaccade from cue onset to 0.5s post
690   stimulus onset (d). Solid lines indicate medians. The results in d demonstrate that
691   even with no microsaccades preceding the observed modulation, neurons in
692   fSTS show attention-related modulation that is dependent on SC activity.

693 e-f. Same format as c-d, but attention-related modulation was computed in the
694   standard time window (1-1.5s, magenta box under x-axis in a, b) using the same
695   trials as in c, d. We present these data in order to directly relate this analysis with
696   the analyses reported in the main text, which uses the 1-1.5s window (figure 2c),
697   but note that it is still possible that microsaccades occurred after our exclusion
698   window (-0.7 to 0.5s relative to stimulus onset) and before the delay period (1-
699   1.5s post stimulus onset).

700

701

33
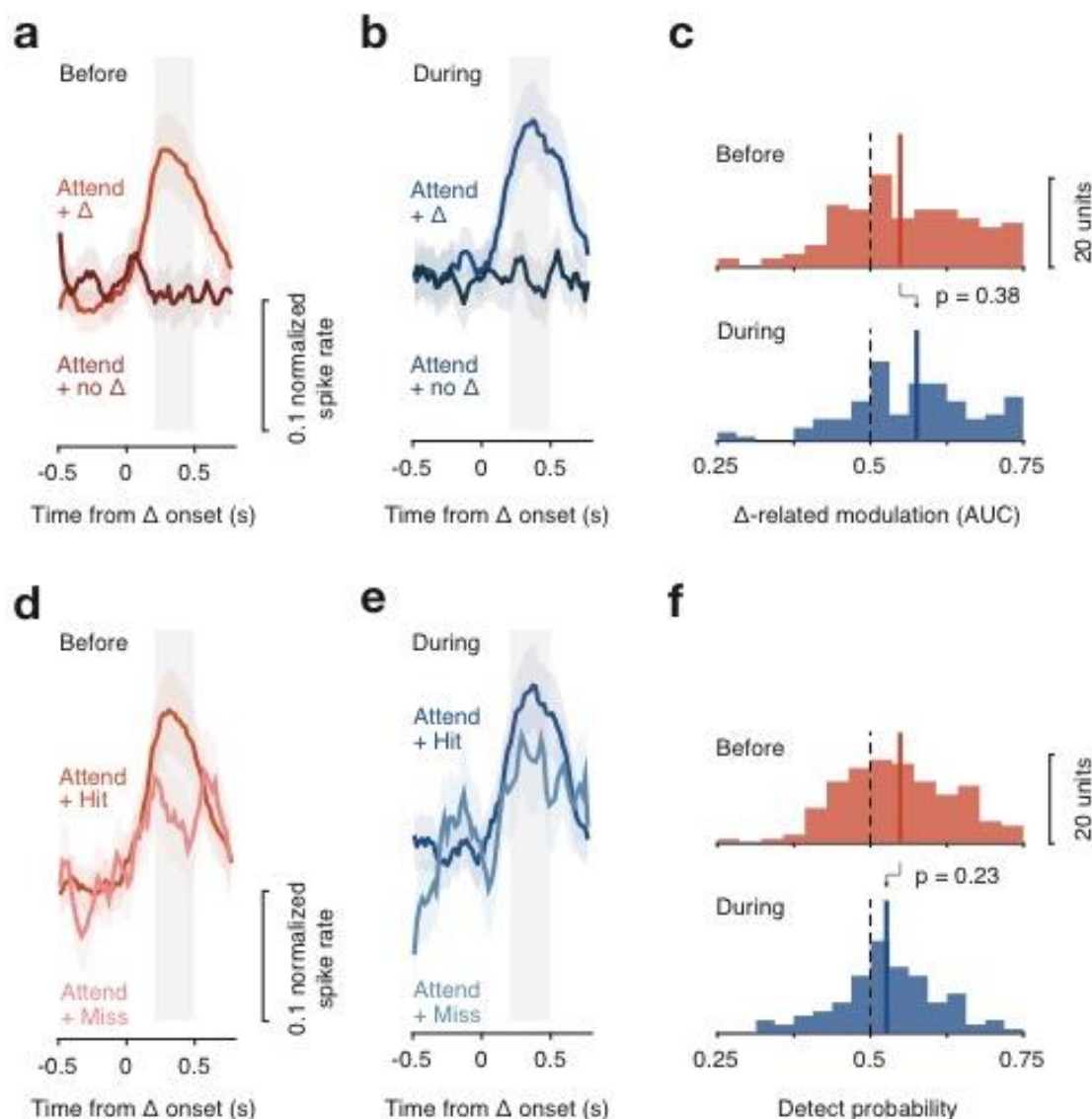
702
703
Supplementary Figure 7. Saline and sham injections had no effect on change-related activity or detect probability in fSTS
a-c. Change related activity before and during saline/sham injections (same format as Figure 3a-c).
d-f. Detect probability before and during saline/sham injections (same format as Figure 3e-g).
710
711
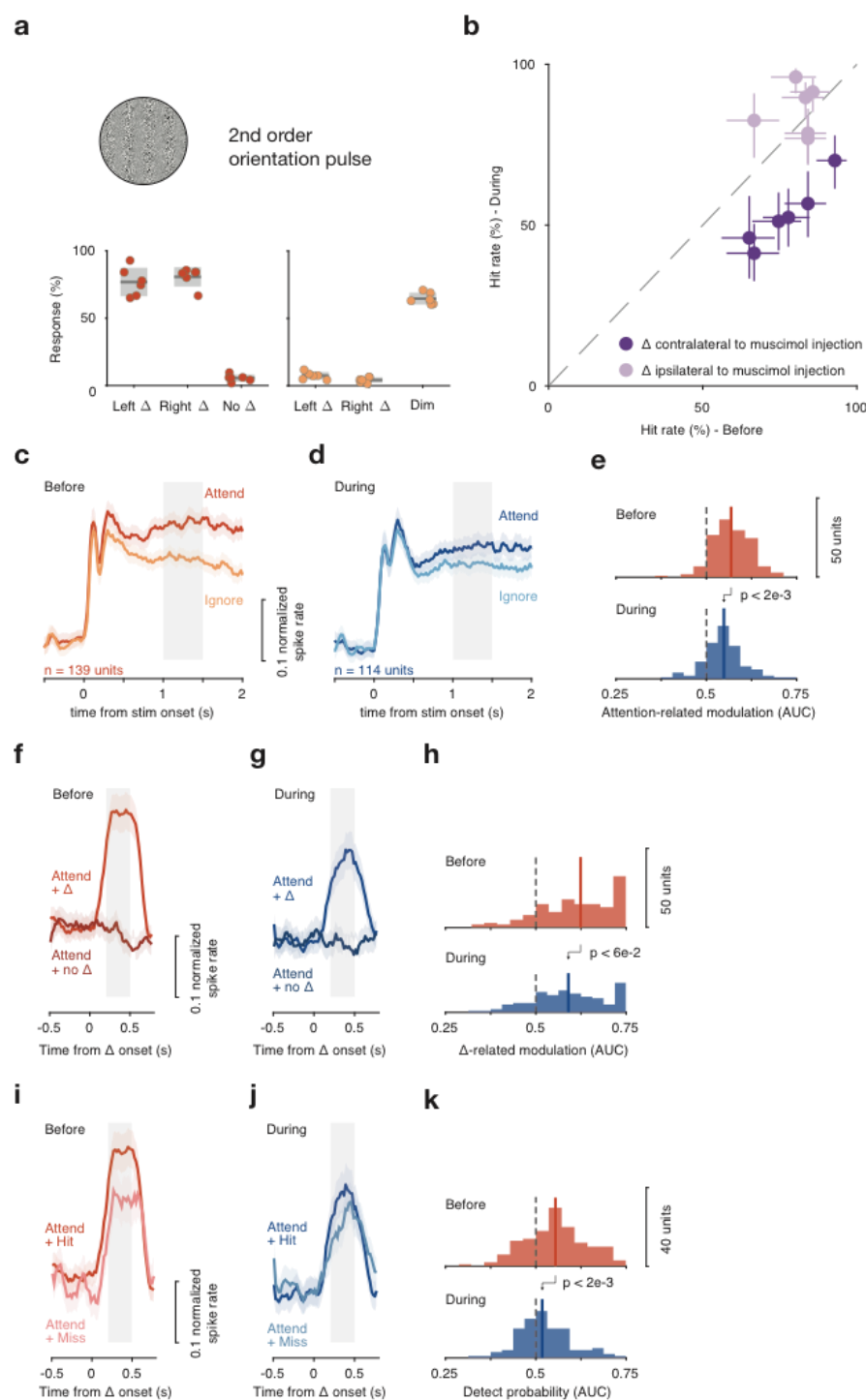
712
713
Supplementary Figure 8. Effect of SC inactivation on attention-related modulation, change-related activity and detect probability in fSTS neurons was not specific to motion stimuli

a. A 2nd order orientation pulse stimulus (that contains no motion energy) was used in 6 SC inactivation sessions to evaluate whether the effects of SC inactivation on fSTS neurons was specific to motion stimulus (see methods). Top: image of

720   orientation pulse. Bottom: behavioral performance in the task (similar format to
721   figure 1a, b).

722 b. A comparison of hit rate (i.e. the successful detection of an orientation pulse) for
723   contralateral and ipsilateral stimuli, in the *Attend* condition, before and during SC
724   inactivation. The observed contralateral deficits with the second-order stimulus
725   are consistent with a previous report [8].

726 c-e. Attention-related modulation before and during SC inactivation (same format as
727   figure 2a-c).

728 f-h. Change-related activity before and during SC inactivation (same format as figure
729   3a-c).

730 i-k. Detect probability before and during SC inactivation (same format as figure 3e-g).

731

732

36
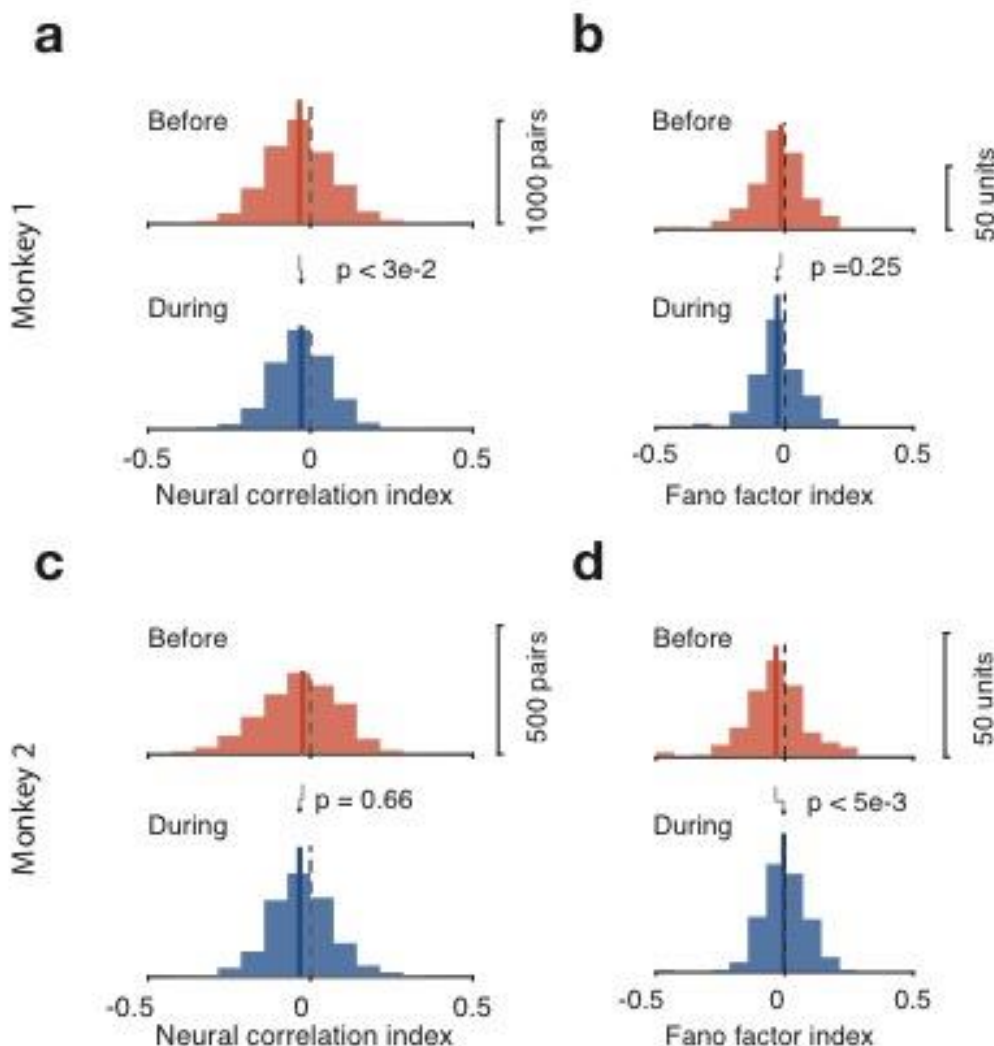
733
Supplementary Figure 9. Effect of SC inactivation on spike count correlations and fano-factor in fSTS neurons

a. Distribution of neuronal correlation indices (see Methods) before (top) and during (bottom) SC inactivation, for monkey 1.

b. Distribution of neuronal fano-factor indices (see Methods) before (top) and during (bottom) SC inactivation, for monkey 1.

c. Same as a, for monkey 2.

d. Same as b, for monkey 2.
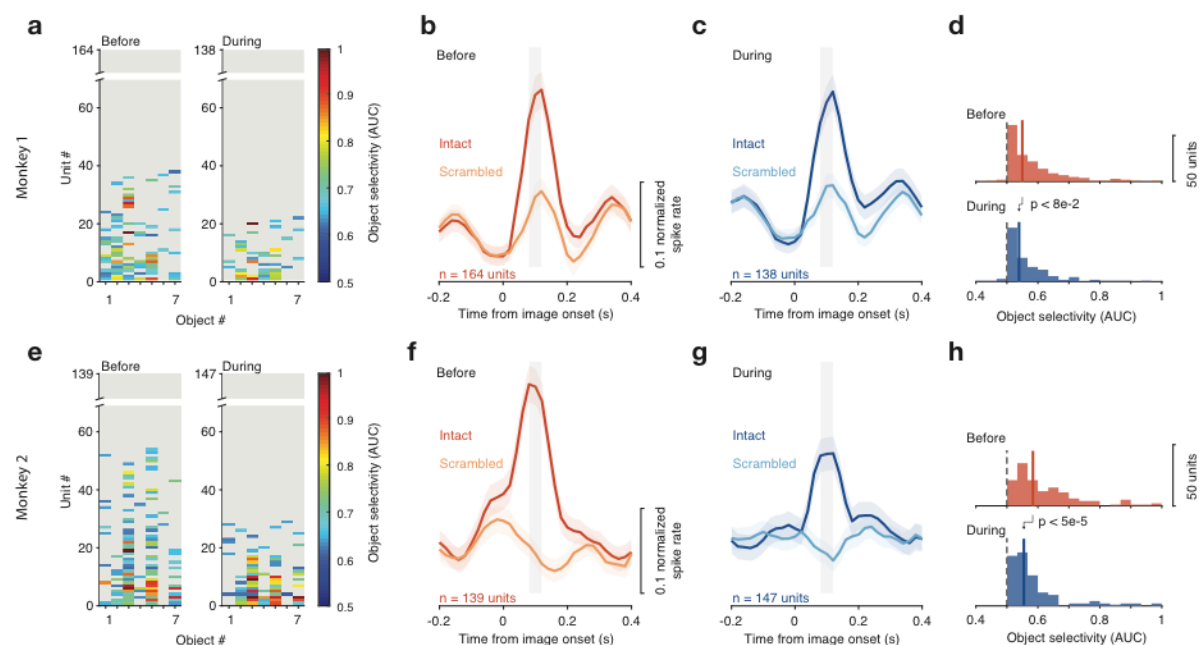
744
745
746 **Supplementary Figure 10. Effect of SC inactivation on object selectivity in fSTS**
747 **neurons is similar across monkeys**
748   a. Object selectivity across single neurons and the population, before and during
749   SC inactivation, in monkey 1 (same format as figure 4c-f).
750   b. Object selectivity across single neurons and the population, before and during
751   SC inactivation, in monkey 2 (same format as figure 4c-f).
752
753
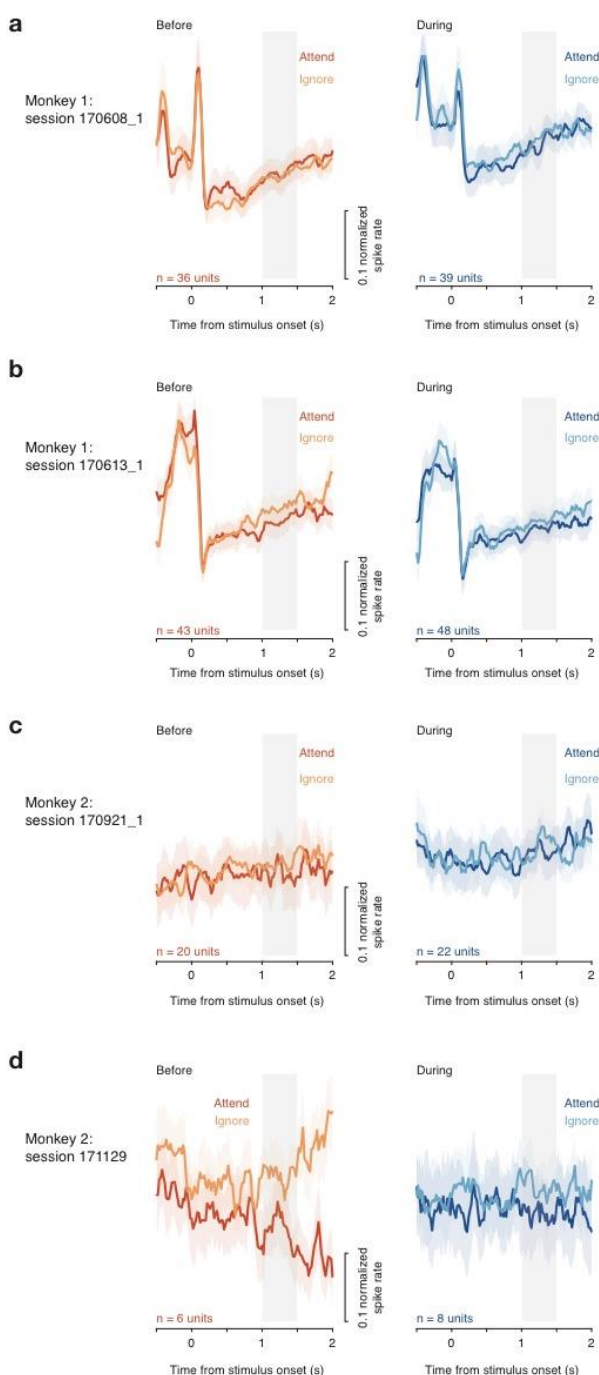
754
755
Supplementary Figure 11. Neurons outside of the circumscribed fMRI 'hotspot' show non-standard responses

a-d. Population average of neuronal responses, recorded in locations outside of the putative hotspot (monkey 1: a, b; monkey 2: c, d), to motion stimulus in the *Attend* and *Ignore* conditions, before (left) and during (right) SC inactivation.

761

39